Lattice Boltzmann model for melting with natural convection

Christian Huber [a,*], Andrea Parmigiani [b], Bastien Chopard [b], Michael Manga [c], Olivier Bachmann [d]

[a] Department of Earth and Planetary Science, University of California – Berkeley, 307 McCone Hall 4767, Berkeley, CA 94720-4767, USA
[b] Computer Science Department, University of Geneva, 24, Rue du Général Dufour, 1211 Geneva 4, Switzerland
[c] Department of Earth and Planetary Science, University of California – Berkeley, 177 McCone Hall 4767, Berkeley, CA 94720-4767, USA
[d] Department of Earth and Space Science, University of Washington, Johnson Hall 070, Seattle WA 98195-1310, USA

ARTICLE INFO

ABSTRACT

We develop a lattice Boltzmann method to couple thermal convection and pure-substance melting. The transition from conduction-dominated heat transfer to fully-developed convection is analyzed and scaling laws and previous numerical results are reproduced by our numerical method. We also investigate the limit in which thermal inertia (high Stefan number) cannot be neglected. We use our results to extend the scaling relations obtained at low Stefan number and establish the correlation between the melting front propagation and the Stefan number for fully-developed convection. We conclude by showing that the model presented here is particularly well-suited to study convection melting in geometrically complex media with many applications in geosciences.

© 2008 Elsevier Inc. All rights reserved.

1. Introduction

Melting caused by natural convection occurs in many settings, from large-scale phenomena in geosciences to small-scale industrial processes during alloy solidification and crystal growth. Models of convection melting need to account for thermally-driven flow coupled with a moving interface where latent heat is either absorbed (melting) or released (solidification). The interplay between the fluid flow and the moving boundary leads to a complex dynamical behavior, as the position of the solid liquid interface becomes one of the unknowns of the problem (Jany and Bejan, 1988). The variables of interest are the melting front position and the Nusselt number, which describe, respectively, the evolution of the geometry of the system and the heat transfer. The moving boundary problem usually requires complex numerical schemes such as front tracking methods (Bertrand et al., 1999), adaptative grid methods (Mencinger, 2004), level set methods (Tan and Zabaras, 2006), phase field approaches (Boettinger et al., 2002) or volume-of-fluid methods (Hirt and Nichols, 1981).

Natural convection melting has been investigated by numerous experimental (Bénard et al., 2006; Wolff and Viskanta, 1987; Dong et al., 1991; Hirata et al., 1993; Wang et al., 1999), theoretical (Viskanta, 1982; Viskanta, 1985; Jany and Bejan, 1988; Zhang and Bejan, 1989) and numerical studies (Webb and Viskanta,

1986; Bertrand et al., 1999; Mencinger, 2004; Usmani et al., 1992; Chatterjee and Chakraborty, 2005; Javierre et al., 2006). The development of appropriate scaling laws (e.g. Jany and Bejan, 1988) and powerful computational methods have significantly improved the understanding of the convection melting processes. Heat transfer correlations for the Nusselt number have been developed, but the range of values for the key dimensionless groups (Rayleigh, Prandtl and Stefan numbers) over which the correlations have been tested remains limited.

The lattice Boltzmann method, developed over the last two decades, provides a powerful alternative approach for studying convection involving phase changes. Compared with classic computational fluid dynamics methods, it offers two significant advantages. First, no-slip boundary conditions in complex geometries can be implemented through simple local rules (Chopard and Droz, 1998). Second, the main part of the algorithm is purely local, making the LB method straightforward to parallelize even though not necessarily more efficient than for example the "continuum" finite difference method (Nourgaliev et al., 2000, 2003).

In this study we develop a Lattice Boltzmann (LB) method to model pure substance conduction and convection melting. We start by introducing the mathematical description of the problem together with previously established scaling laws (Jany and Bejan, 1988) for the convection case. We then introduce the LB method, with extensions for the thermal model (using a multiple distribution approach) and the phase transition (using a modified version of Jiaung et al. (2001) algorithm). In Section 4, we compare the results of our model with analytical solutions (for the conduction case) and with the scaling laws obtained by Jany and Bejan

* Corresponding author.
E-mail addresses: chuber@seismo.berkeley.edu (C. Huber), andrea.parmigiani@terre.unige.ch (A. Parmigiani), Bastien.Chopard@cui.unige.ch (B. Chopard), manga@seismo.berkeley.edu (M. Manga), bachmano@u.washington.edu (O. Bachmann).

(1988) for the convection problem. We extend their scaling laws to high Stefan numbers (i.e. where thermal inertia is non-negligible) for the Nusselt number and the position of the melting front. Finally, we show that the model developed here is able to handle non-idealized problems with complex geometries such as porous media with no additional complications.

2. Review of pure substance melting

The problem of half space conduction melting with homogeneous, isotropic thermal diffusivity, has been solved analytically in 1860 by Neumann. Heat transfer in the liquid is given by

$$\frac{\partial T}{\partial t} = \kappa \nabla^2 T, \tag{1}$$

where T is temperature, and κ the thermal diffusivity. Nomenclature is summarized in Table 1. At the melt-solid boundary, when the solid is kept at the melting temperature, the energy balance requires that

$$\kappa \left(\frac{\partial T}{\partial x} \right)_{x=x_m} = \frac{L_f}{c} \frac{dx_m}{dt}. \tag{2}$$

Here, c is the heat capacity, x_m is the position of the melting front and L_f the latent heat of fusion (see Fig. 1a). The problem is often recast by separating enthalpy in a sensible heat and a latent heat term (Faghri and Zhang, 2006),

$$\frac{\partial T}{\partial t} = \kappa \nabla^2 T - \frac{L_f}{c} \frac{\partial f_l}{\partial t}, \tag{3}$$

where f_l is the melt fraction; or in dimensionless form,

$$\frac{\partial T^*}{\partial t^*} = \nabla^2 T^* - \frac{1}{St} \frac{\partial f_l}{\partial t^*}, \tag{4}$$

where the dimensionless scalings are $T^* = (T - T_0)/(T_1 - T_0)$; $x^* = x/l$, l is the natural length scale of the system; $t^* = t\kappa/l^2$. T_1, T_0 are, respectively, the temperature of the superheat applied within the liquid and the initial temperature of the solid (or, in the case of no undercooling, the melting temperature). St is the Stefan number, $St = c(T_1 - T_0)/L_f$. It is important to note that Eq. (1) together with Eq. (2) are exactly equivalent with Eq. (3). Whereas the first version ensures thermal energy balance at the interface through a boundary condition, the second introduces the latent heat contribu-
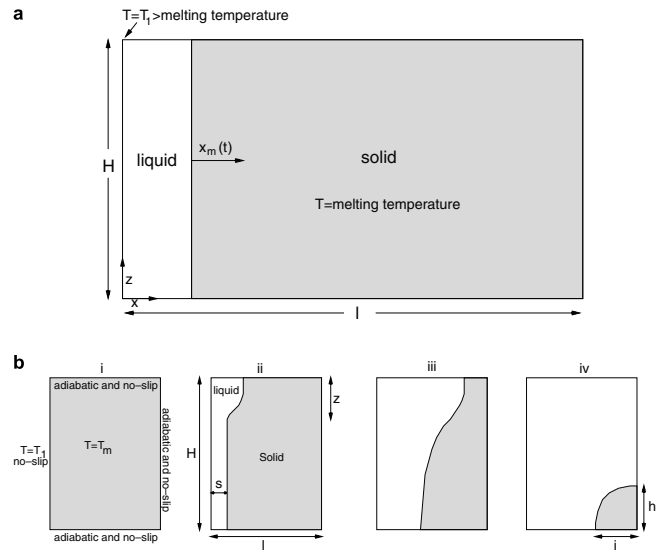
Table 1
Nomenclature

c	specific heat of the liquid phase
c_1	fitting parameter for Nu–Fo correlation
c_2	fitting parameter for Nu–Fo correlation
En	enthalpy
En_s	enthalpy of the solid phase at the melting temperature
En_l	enthalpy of the liquid phase at the melting temperature
f_l	liquid fraction
Fo	Fourier number $= \kappa t/H^2$
g	acceleration due to gravity
H	height of enclosure
l	width of the enclosure
L_f	latent heat of fusion
Nu	Nusselt number
p	pressure
Pr	Prandtl number $= \nu/\kappa$
Ra	Rayleigh number $= g\beta(T_1 - T_0)H^3/(\kappa\nu)$
St	Stefan number $= c(T_1 - T_0)/L_f$
T_1	temperature of the superheat applied to the liquid
T_0	temperature of the solid (here melting temperature)
β	coefficient of thermal expansion
κ	thermal diffusivity of the fluid
λ	coefficient depending on St (Eq. (5))
ν	kinematic viscosity

Fig. 1. (a) Schematic representation of the conduction melting problem. (b) Schematic representation of the different stages of the convection melting problem. The solid is initially at the melting temperature T_m: (i) boundary conditions; (ii) conduction and convection; (iii) convection dominated; (iv) after the melting front reached the right boundary.

tion in the diffusion equation as a sink term. As a result, when the latter is discretized, a careful choice of time step is required in order to ensure energy conservation at the interface otherwise the sink term can prevail over the heat transport and lead to non-physical behavior (see Section 3.2).

For a system starting with zero undercooling (the solid is initially at the melting temperature), Neumann found that the solution in the liquid half-space is given by

$$T(x,t) = T_1 - (T_1 - T_0) \frac{\text{erf}(x/(2\sqrt{\kappa t}))}{\text{erf}(\lambda)}, \quad \text{for } 0 \leqslant x \leqslant x_m(t),$$
$$x_m(t) = 2\lambda\sqrt{\kappa t}, \tag{5}$$
$$\lambda \exp(\lambda^2)\text{erf}(\lambda) = \frac{St}{\sqrt{\pi}},$$

where x_m is the melting front position.

Using the same set of dimensional scales, the system of equations for convection melting, in the case of Newtonian incompressible fluids under the Boussinesq approximation (and neglecting viscous heating), can be written as Bodenschatz et al. (2000)

$$\nabla \cdot \mathbf{u}^* = 0, \tag{6}$$
$$\frac{\partial \mathbf{u}^*}{\partial t^*} + \mathbf{u}^* \cdot (\nabla \mathbf{u}^*) = -\nabla p^* + Pr\nabla^2\mathbf{u}^* - PrRa\beta T^*, \tag{7}$$
$$\frac{\partial T^*}{\partial t^*} + \mathbf{u}^* \cdot \nabla T^* = \nabla^2 T^* - \frac{1}{St} \frac{\partial f_l}{\partial t^*}, \tag{8}$$

where $Pr = \nu/\kappa$ is the Prandtl number and $Ra = g\beta\Delta T l^3/(\kappa\nu)$ is the Rayleigh number, ν, β and g are, respectively, the kinematic viscosity, the thermal expansion and the acceleration due to gravity and l is an appropriate length scale for the problem (l will correspond to the height of the enclosure for the convection melting problem).

Owing to their non-linear behavior the equations for convection melting cannot be solved analytically and require numerical integration. However, for simple geometries and flow behavior (low Reynolds numbers, Boussinesq approximation), Jany and Bejan (1988) showed that using appropriate representative lengthscales, it is possible to infer scaling relationships for the evolution of the system. These scaling laws have been successfully tested both numerically (Webb and Viskanta, 1986; Jany and Bejan, 1988; Bertrand et al., 1999) and experimentally (Bénard et al., 2006; Wolff

and Viskanta, 1987; Gobin and Bénard, 1992; Wang et al., 1999). However, owing to the difficulty of experiments in satisfying perfectly isothermal or adiabatic walls and no density change induced by the phase transition, we decide to validate our numerical model with the scaling laws of Jany and Bejan (1988) and the benchmark exercise of Bertrand et al. (1999). Fig. 1b shows the boundary conditions and the different stages for the melting of a 2D rectangular cavity of height H.

The first stage is dominated by heat conduction melting, although owing to the vertical geometry of the cavity, sluggish convection will take place because of the horizontal temperature differences in the thin fluid layer. During this stage, Jany and Bejan showed that the Nusselt number is

$$Nu \propto \theta^{-1/2} + Ra\ \theta^{3/2}, \tag{9}$$

where $\theta = Fo\,St$, $Fo = \kappa t/l^2$ is the Fourier number, and $Ra = g\beta(T_1 - T_0)H^3/(\kappa\nu)$. This stage ends when the convection zone thickness z (see Fig. 1b-iii) extends to the height of the cavity. The dimensionless time θ_1 at which this occurs was found to be related to the Rayleigh number according to the law

$$\theta_1 \propto Ra^{-1/2}. \tag{10}$$

Finally, the scaling predicts that the Nusselt number will evolve to a minimum

$$Nu_{min} \propto Ra^{1/4}, \tag{11}$$

occurring close to the end of this regime.

In the convection regime ($z = H$), the Nusselt number reaches a plateau at

$$Nu \propto Ra^{1/4}. \tag{12}$$

The height-averaged position of the melting front s_{av} and the dimensionless time at which melting reaches the right boundary of the domain θ_2 are given by

$$s_{av} = \frac{1}{H} \int_0^H x_m \, dz \propto HRa^{1/4}\theta \tag{13}$$

and

$$\theta_2 = \frac{l}{H} Ra^{-1/4}, \tag{14}$$

where l is the horizontal dimension of the cavity. Finally, Jany and Bejan (1988) showed that the scaling results listed above are valid at high Prandtl number ($Pr > O(1)$) and proposed to rescale $Ra \rightarrow Ra\,Pr$ when $Pr < 1$ in every scaling law.

3. Lattice Boltzmann (LB) model

In the LB model, the fluid is described by quantities f_i representing the particle density distributions in the ith velocity direction of the lattice;

$$f_i = f_i(\mathbf{x}, t), \quad i = 0, \dots, M, \tag{15}$$

where $\mathbf{x}$ is the position on the lattice and t the time. M represents the number of velocity directions of the particles at each node of the lattice. The volumetric mass ρ and the momentum $\rho\mathbf{u}$ are defined as particle velocity moments of the distribution function (Frisch et al., 1986)

$$\rho = \sum_{i=0}^{M} f_i, \quad \rho\mathbf{u} = \sum_{i=1}^{M} f_i \mathbf{e}_i, \tag{16}$$

where $\mathbf{e}_i$ is the local particle velocity. In the single relaxation time (or LBGK) model, the equation for f_i is (Qian et al., 1992; Chopard and Droz, 1998)

$$f_i(\mathbf{x} + \mathbf{e}_i, t + 1) = f_i(\mathbf{x}, t) - \frac{1}{\tau}(f_i(\mathbf{x}, t) - f_i^{eq}(\mathbf{x}, t)). \tag{17}$$

In this relation, the relaxation parameter τ expresses the rate at which the local particle distribution relaxes to the local equilibrium state f_i^{eq}.

Let us consider a two-dimensional regular grid with a nine-velocity lattice (the so-called D2Q9 topology) (Wolf-Gladrow, 2000). The velocities $\mathbf{e}_i$ are given by

$$\mathbf{e}_i = \begin{cases} (0,0) & i = 0, \\ (\cos((i-1)\pi/2), \sin((i-1)\pi/2)) & i = 1,2,3,4, \\ \sqrt{2}(\cos((2(i-5)+1)\pi/4), \sin((2(i-5)+1)\pi/4)) \\ \quad i = 5,6,7,8. \end{cases} \tag{18}$$

In this case, the equilibrium distribution function may be written as

$$f_i^{eq} = \rho w_i \left[1 + 3(\mathbf{e}_i \cdot \mathbf{u}) + \frac{9}{2}(\mathbf{e}_i \cdot \mathbf{u})^2 - \frac{3}{2}\mathbf{u} \cdot \mathbf{u} \right] \tag{19}$$

with $w_0 = 16/36$, $w_i = 4/36$ for $i = 1,2,3,4$ and $w_i = 1/36$ for $i = 5,6,7,8$. With the appropriate equilibrium distribution, and defining the speed of sound as $c_s^2 = c^2/3$, we can recover the continuity and Navier–Stokes equations through a Chapman–Enskog expansion (Frisch et al., 1986; Qian et al., 1992; Chopard and Droz, 1998). Accordingly, the pressure p is identified with $p = \rho c_s^2$ and the kinematic viscosity (in lattice units) is defined by

$$\nu = c_s^2 \, dt(\tau - 0.5) \tag{20}$$

where dt is the timestep. The positivity of the viscosity requires $\tau > 0.5$. For more details about the algorithm, the reader is referred to lattice Boltzmann textbooks (Chopard and Droz, 1998; Succi, 2001; Wolf-Gladrow, 2000).

3.1. Thermal lattice Boltzmann

When the latent heat term is neglected, Eq. (8) becomes the standard advection–diffusion equation for temperature

$$\frac{\partial T^*}{\partial t^*} + \mathbf{u}^* \cdot \nabla T^* = \nabla^2 T^*. \tag{21}$$

The existing LB models developed for thermal flows can be classified into four categories: multispeed (MS), entropic, hybrid and multi-distribution function (MDF) models.

The MS approach (McNamara and Alder, 1993a,b) is a straightforward extension of the isothermal LBGK model in which only one particle distribution function f_i is used to recover the entire set of thermo-hydrodynamics equations. Density, momentum and internal energy conservation are obtained from the moments of the distribution f_i. For computational efficiency, the lattice topology is chosen so as to minimize the number of discrete velocities for which the LB model recovers the macroscopic dynamics of interest. In order to recover the desired set of equations (conservation laws), a thermal MS model needs a larger number of lattice velocities compared to an isothermal LBGK model. One of the obvious restrictions of using a single LBGK model for thermal problems is the impossibility of varying the Prandtl number.

Prasianakis and Karlin (2007) have developed a single distribution thermal LB scheme with variable Prandtl number on standard lattices (e.g., D2Q9 for a 2D model). They use an entropic lattice Boltzmann scheme (Ansumali and Karlin, 2002) for which a correction term recovers the Navier–Stokes equation (in the compressible regime), the advection–diffusion equations for temperature, and also provides a free parameter for tuning the Prandtl number. However, the correction term is non-local. Hybrid models couple the flow field calculated with a conventional LB scheme with finite differences or finite elements to solve for the heat equation (Lallemand and Luo, 2003; Mezrhab et al., 2004).

In the present study, we choose the MDF approach (Shan, 1997; Guo et al., 2002) to model natural convection. The thermal advection–diffusion Eq. (21) is solved by introducing a second distribution function (g_i) whose evolution is also described by a LBGK dynamic. The two distributions are coupled through the buoyancy term for f_i, and the equilibrium distribution for g_i,

$$f_i(\mathbf{x} + \mathbf{e}_i, t+1) = f_i(\mathbf{x}, t) - \frac{1}{\tau}(f_i(\mathbf{x}, t) - f_i^{eq}(\mathbf{x}, t)) + \hat{\mathbf{g}}$$
$$\cdot \, \mathbf{e}_i Pr\, Ra\, T(t)/\Delta T, \qquad (22)$$

$$g_i(\mathbf{x} + \mathbf{v}_i, t+1) = g_i(\mathbf{x}, t) - \frac{1}{\tau_h}(g_i(\mathbf{x}, t) - g_i^{eq}(\mathbf{x}, t)). \qquad (23)$$

The LBGK model for g_i is similar to Eq. (17) but a simplified equilibrium distribution function can be used:

$$g_i^{eq} = T w_i^T [1 + \frac{1}{C_{sh}^2}(\mathbf{v}_i \cdot \mathbf{u})], \qquad (24)$$

where v_i and w_i^T are the associated lattice velocities and weights, and $\mathbf{u}$ is the macroscopic fluid flow velocity. Eqs. (23) and (24) are first order approximations, therefore, correcting terms have to be used to make it second order accurate (Lätt, 2007). The MDF approach allows us to use two different lattices for the two distribution functions. For the evolution of g_i, given its simplified equilibrium distribution function, a D2Q5 lattice is preferred. In the D2Q5 topology, the velocities v_i are

$$\mathbf{v}_i = \begin{cases} (0,0) & i = 0, \\ (\cos((i-1)\pi/2), \sin((i-1)\pi/2)) & i = 1,2,3,4. \end{cases} \qquad (25)$$

The associated weights w_i^T are $w_0^T = 1/3, w_i^T = 1/6$ for $i = 1,2,3,4$. At each lattice node, the macroscopic temperature is defined as

$$T = \sum_{i=0}^{4} g_i \qquad (26)$$

and the thermal diffusivity (in lattice units) is related to the relaxation time

$$\kappa = C_{sh}^2 \, dt(\tau_h - 0.5). \qquad (27)$$

The MDF approach offers the possibility to vary the Prandtl number by adjusting the two relaxation times τ and τ_h

$$Pr = \frac{(2\tau - 1)}{(2\tau_h - 1)}. \qquad (28)$$

3.2. Phase change with lattice Boltzmann

Different LB approaches have been proposed for solid–liquid phase transitions. They can be grouped in two methods: (1) the phase-field method using the theory of Ginzburg–Landau (Miller and Succi, 2002; Rasin et al., 2005; Medvedev and Kassner, 2005); (2) enthalpy-based methods (Jiaung et al., 2001; Chatterjee and Chakraborty, 2005). We use a sightly modified version of the Jiaung et al. (2001) melting scheme for the conduction case, using a D2Q5 topology. Jiaung et al. use an iterative enthalpy-based method to solve for both the temperature and melt fraction fields at each time step. The melting term is introduced as a source (crystallization) or sink (melting) term in the collision step. In summary, at the timestep n, iteration k, the macroscopic temperature is calculated

$$T^{n,k} = \sum_{i=0}^{4} g_i^{n,k}, \qquad (29)$$

where $T^{n,k} \equiv T^k(t=n)$. The local enthalpy is obtained by

$$En^{n,k} = cT^{n,k} + L_f f_l^{n,k-1} \qquad (30)$$

with the liquid fraction f_l of the previous iteration. Finally, the enthalpy is used to linearly interpolate the melt fraction

$$f_l^{n,k} = \begin{cases} 0 & En^{n,k} < En_s = cT_m, \\ \frac{En^{n,k} - En_s}{En_l - En_s} & En_s \leqslant En^{n,k} \leqslant En_s + L_f, \\ 1 & En^{n,k} > En_s + L_f. \end{cases} \qquad (31)$$

The collision is then calculated

$$g_i^{n,k+1}(\mathbf{x} + \mathbf{e}_i) = g_i(\mathbf{x}) - \frac{1}{\tau_h}(g_i(\mathbf{x}) - g_i^{eq}(\mathbf{x})) - w_i \frac{L_f}{c}(f_l^{n,k}(\mathbf{x}) - f_l^{n-1}(\mathbf{x})), \qquad (32)$$

until the temperature and the melt fraction field converge to within a set tolerance. The timestep $n+1$ is calculated using the same procedure. Jiaung et al. (2001) obtain accurate solutions for $O(10^{-1}) \leqslant St \leqslant O(1)$ and a relaxation time $\tau_h = 1$. For the sake of efficiency, we modified the scheme and set the number of iterations to $k = 1 \forall n$ at the expense of the accuracy. However, we performed tests revealing that, over the range of parameters used in this study, setting $k = 1$ has negligible effects, but becomes valuable for the computationally intensive convection melting problems.

As the Jiaung et al. (2001) scheme is a LB version of Eq. (3), we show that special attention must be given to the choice of parameters used in the numerical calculations. Using the total time of the run t_{max} as the timescale, we get a new non-dimensional version of the differential equation

$$\frac{\partial T^*}{\partial t^*} = \frac{\kappa t_{max}}{l^2} \nabla^2 T^* - \frac{1}{St} \frac{\partial f_l}{\partial t^*}. \qquad (33)$$

Eq. (33) shows that for a melting event the temperature evolution is subject to a source term (the heat transported from the hot wall) and a sink term (the heat consumed by the phase change). When $\kappa t_{max}/l^2 < cnst St^{-1}$, the sink term dominates and the temperature can locally decrease below the initial solid temperature, in contradiction with the phase change associated with pure substance melting. Therefore the choice of spatial and temporal discretization is important (will modify $\kappa t_{max}/l^2$), especially at low thermal diffusivity. Accordingly, we modified the collision step to ensure no heat transfer in parts of the domain where the enthalpy has remained equal to the initial enthalpy of the solid. This is done by applying the collision as in Jiaung et al. (2001) for every site $\mathbf{x}$ where the enthalpy $En(\mathbf{x}) > cT_{ini}$ and using bounceback for the remaining sites. This is equivalent to forcing the boundary condition of Eq. (2) in the Jiaung et al. scheme. As a result, the temperature field obtained numerically is in better agreement with theory, especially when using small relaxation times ($0.5 < \tau_h < 1$) and a small number of time steps.

On the other hand, if the Stefan number is high compared with $\kappa t_{max}/l^2$, there will be a limit at which the scheme cannot solve the evolution of the melting front. The condition is that the melting front velocity dx_m/dt does not exceed the lattice speed dx/dt. Using Eqs. (5) and (27), in lattice units, this condition translates to

$$\tau_h < 0.5 + 3\frac{1}{\lambda^2}, \qquad (34)$$

which gives approximately $\tau_h < 3.5$ and $\tau_h < 48.5$ for, respectively, $St = 10$ and $St = 0.1$. In Eq. (34), λ is given by Eq. (5).

For the convection melting problem, we develop a new scheme based on the thermal lattice Boltzmann model described in Section 3.1. The two distributions are coupled through the buoyancy force and the equilibrium distribution g_i^{eq} (for the advection term). An additional coupling arises from the melting scheme through the melting front position determined by the temperature scheme.

When a site becomes liquid, the distribution functions f_i's are initialized with the equilibrium values with a reference density and a zero velocity (because of the no-slip boundary condition). We also used a velocity extrapolated from the neighboring fluid sites, and found no notable differences. The collision step for the fluid distribution is modified accordingly, and we perform the standard collision of Eq. (17) at every site where the liquid fraction is above 0.5 (this choice is arbitrary and represents the limit at which most of the voxel of the given site is in the fluid state) and bounceback everywhere else. For the wall boundary conditions, bounceback is applied on the four walls for the fluid distribution. For the sake of simplicity, especially for complex geometries, we use on-grid bounceback and define the solid–liquid interface to be located at mid-grid to recover second order accuracy. Upper, lower and right walls are adiabatic (no heat flow out) and are implemented through the bounceback of the temperature distribution (Kumar et al., 1999; van der Sman, 2004, 2006). We tested the bounceback of the temperature distribution against a second order finite difference approximation for the adiabatic boundaries and we found a good agreement (no difference for the Nusselt number and within a percent of each other for the average melting front position when it reached the half width of the enclosure). Finally, the left wall is set at a fixed temperature T_1 by setting the only unknown g_1 to

$$g_1 = T_1 - (g_0 + g_2 + g_3 + g_4) \qquad (35)$$

for all sites on the left wall.

We emphasize that the choice $\kappa_{\mathrm{solid}} = \kappa_{\mathrm{liquid}}$ is not a necessary condition and that the viscosity can be set to be a function of the temperature by rescaling the relaxation time of the fluid distribution τ accordingly (Guo and Zhao, 2005). The two latter extensions will not be discussed in this study, but are important for actual applications. Lastly, the scheme presented here is not fully incompressible; for convection melting problems at higher Mach numbers, the incompressible model of Guo et al. (2000) is required.

4. Results and discussion

In this section we present the results of both conduction and convection melting with our lattice Boltzmann model and compare them with analytical solutions (for the conduction case) and with the scaling obtained by Jany and Bejan (1988).

4.1. Conduction melting

The different results obtained for conduction melting (the Stefan problem) are summarized in Figs. 2–4. We use a 100×5 grid for all runs. The geometry and boundary conditions are illustrated in Fig. 1a. Fig. 2a shows the melting front position as function of time for three different thermal diffusivities $\kappa = 0.033, 0.36$ and 0.7 in lattice units, corresponding to relaxation times τ of 0.6, 1.6 and 2.6, respectively, with a fixed Stefan number of $St = 1$. Fig. 2b shows the temperature distributions at the end of each run (corresponding to 10,000 time steps) shown in Fig. 2a. The result of each of these simulations is compared with their respective analytical solutions (Eq. (5)). For both melting front position and temperature, the numerical and analytical results are in good agreement. However, as expected, the fit is better at low thermal diffusivity for our explicit scheme, which, for a fixed grid spacing, is equivalent to smaller time steps, or, for fixed time steps, is equivalent to a better spatial resolution.

Fig. 3 shows the effect of the temporal resolution and the Stefan number on the results obtained for both melting front position and temperature. For each figure, we chose three relaxation times (0.6, 1.6 and 2,6) and ran for the same dimensionless time $t^* = t\kappa/l^2$. Again, the results are in good agreement with the analytical solutions. However, the runs corresponding to the highest thermal dif-
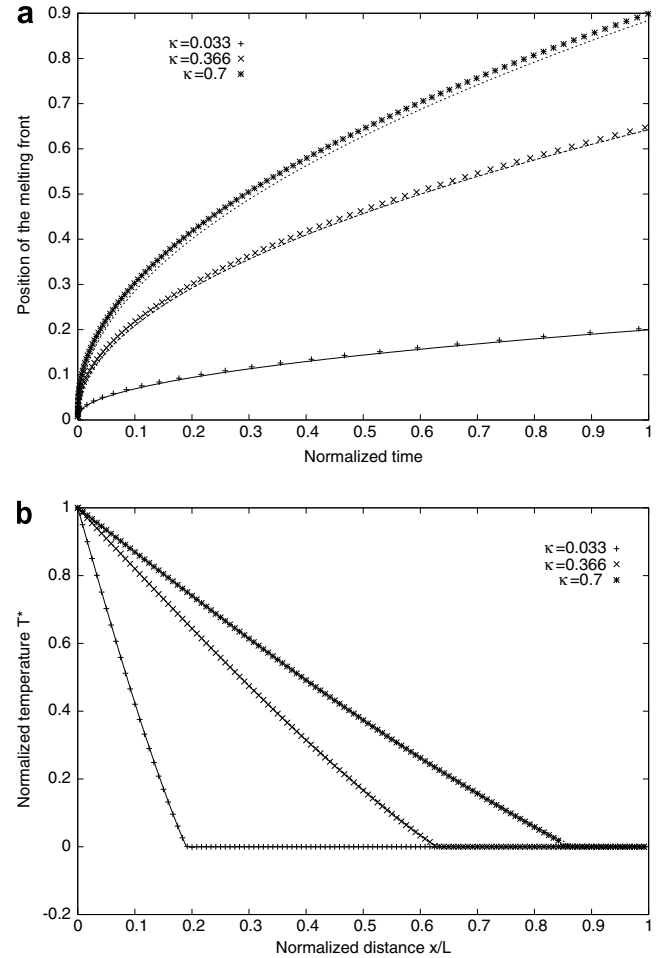

Fig. 2. Comparison of the evolution of the melting front position (a), and the temperature distribution after 10,000 iterations (b) in the conduction case for three different thermal diffusivities and their respective analytical solutions (lines) from Eq. (5), with Stefan number $St = 1$.

fusivity ($\kappa = 0.7$), i.e. the runs with the worst temporal resolution (at least 10 times fewer iterations), resolve the interface less accurately. The variation of the Stefan number over two orders of magnitude does not change the aptitude of the explicit algorithm to solve the Stefan problem.

We can define the error for the temperature distribution and the melting front position to be, respectively

$$\delta T = \frac{\sum_{i=0}^{n_x-1} |T(x_i,t) - T^{\mathrm{th}}(x = x_i,t)|}{\sum_{i=0}^{n_x-1} T^{\mathrm{th}}(x = x_i,t)} \quad \text{and} \qquad (36)$$

$$\delta x_m(t) = \frac{|x_m(t) - x_m^{\mathrm{th}}(t)|}{x_m^{\mathrm{th}}(t)}, \qquad (37)$$

where the superscript 'th' refers to the analytical solution.

Fig. 4a shows the evolution of the relative melting front position error with time for a Stefan number of 0.13. The error in the melting front position decreases rapidly to reach of few percents after $t^* = 0.2$. As expected, the results get better with better temporal resolution. The same feature is observed for the error in the temperature distribution δT of Fig. 4b. Finally, we investigate the dependence of the error in the Stefan number. Figs. 4c and d show that the error on the melting front position decreases with increasing St. This result is expected as the possible error introduced by the explicit algorithm to solve for the non-linear term of Eq. (4) is multiplied by St^{-1} and consequently decreases as the Stefan
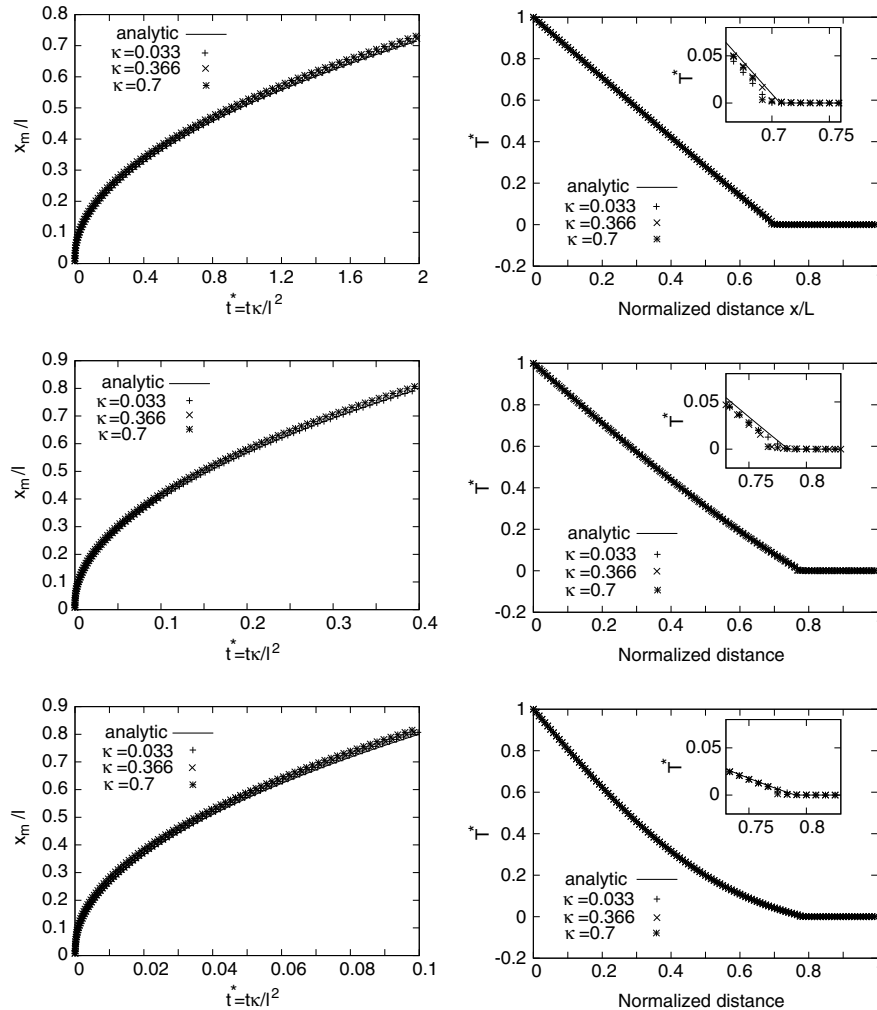
Fig. 3. Comparison of the melting front position and temperature profiles for the same three thermal diffusivities with Stefan number $St = 0.13$ (first row), $St = 1$ (second row) and $St = 10$ (third row). Time is made dimensionless in order to compare the sensitivity of the model to the size of the timesteps.

number increases. Mathematically, in the limit $St \rightarrow \infty$ we recover a simple single phase heat conduction equation from Eq. (4).

4.2. Convection melting

Convection simulations were performed for a square geometry, with the number of lattice points fixed by the value of the desired Rayleigh number and the constraints for stability mentioned in Section 3. The grid sizes range from 75×75, for $Ra = 5 \times 10^4$, to 250×250, for $Ra = 6.8 \times 10^6$. Fig. 5 shows a grid resolution test for $Ra = 25000$, $Pr = 0.02$ and $St = 0.01$ using three different grid sizes. The three results are in very good agreement with Bertrand et al. (1999).

We compared our results with the benchmark of Bertrand et al. (1999) for the case: $Pr = 0.02$, $St = 0.01$, $Ra = 2.5 \times 10^5$. The evolution of the average melting front position and the Nusselt number are in good agreement with the main trend of results showed in Bertrand et al. (1999). The relatively high Nusselt number and oscillatory nature of the results are similar to the results of Le Quéré and Couturier–Sadat listed in Bertrand et al. (1999), where they attribute this behavior to the full transient procedure and the evolution of the circulation cells as melting proceeds.

In this section, we first test our numerical method by recovering the scaling relationships and the correlation coefficients for Nu_{min}, Nu_2, θ_{min} and θ_2 developed by Jany and Bejan (1988) at both low

and high Stefan number $0 \leqslant St \leqslant 10$. Then a comparable run to the one described in Jany and Bejan (1988) ($St = 0.1$, $Pr > O(1)$) is used to reproduce the correlations that were obtained. Second, we show the effect of thermal inertia at high St and compare it to the theory of Jany and Bejan (1988). A review of low Prandtl number effects can be found in Gobin and Bénard (1992), where it was shown that the scaling laws, in this case, have a slight dependence on the Prandtl number.

Fig. 6 shows the evolution of the temperature field in the square cavity as function of time, from the early conduction-dominated stage (upper left) to the fully developed convection (upper right) and finally the entirely melted state (lower right). This run was set with $Ra = 6.8 \times 10^6$, $Pr = 1$ and $St = 10$. The evolution of the melting front is in qualitative good agreement with the expected schematic geometries described in Fig. 1b.

For a more quantitative perspective, we can compare the runs computed for four different Ra ranging from 5×10^4 to 6.8×10^6 with the theoretical predictions obtained from the scaling relationships of Section 2. Fig. 7a shows the evolution of the average melt front position for the four different Ra numbers and the conduction case. As expected the evolution at small θ is controlled by conduction, until more efficient convection increases the melting rate to reach a linear trend during the fully-developed convection regime. Finally the melting rate slows as the melt front reaches the right boundary of the domain. The Nusselt number as function of dimen-
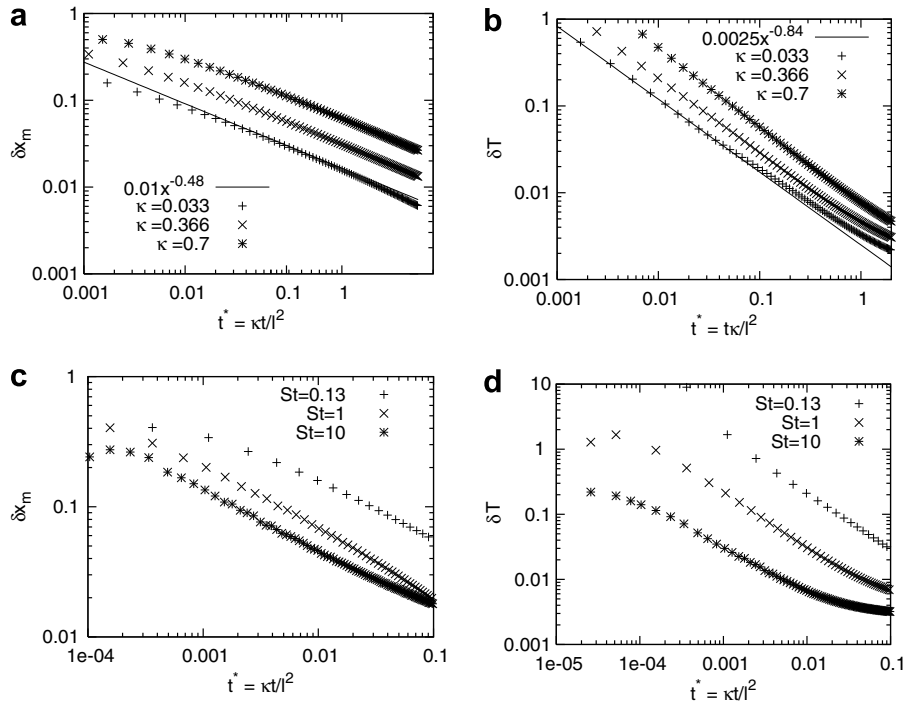
Fig. 4. (a) Relative error on the position of the melting front and on the temperature distribution (b) for the data of Fig. 3 ($St = 0.13$); (c) Relative error on the position of the melting front and on the temperature distribution (d) for $\kappa = 0.366$ and $St = 0.13$, 1 and 10, respectively.
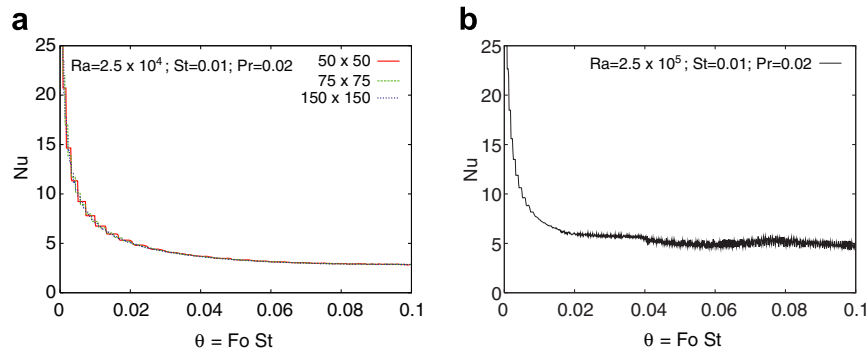

Fig. 5. (a) Resolution tests using three grid sizes 50×50, 75×75 and 150×150. $Ra = 2.5 \times 10^4$, $Pr = 0.02$ and $St = 0.01$. (b) Validation run for $Ra = 2.5 \times 10^5$, $Pr = 0.02$ and $St = 0.01$. The results are similar to the results of Le Quéré and Couturier–Sadat listed in Bertrand et al. (1999). The high Nusselt number and oscillatory behavior of (b) can be explained by the fully transient procedure and small time steps (Bertrand et al., 1999).

sionless time is shown in Fig. 7b for the same four runs. The Nusselt number is computed as in Jany and Bejan (1988)

$$Nu = \int_0^H \frac{\partial T^*}{\partial x^*}(x = 0, z)\, dz. \tag{38}$$

The overall shape of the curves display the expected features described by Jany and Bejan (1988): $Nu \propto \theta^{-1/2}$ at the early stage, and then a minimum followed by a plateau. It is worth noting that the curves here show more time variability than those of Jany and Bejan (1988), especially at high Ra, which can be explained by the low Pr number (=1) used here (higher Reynolds number). We can extract Nu and time of its minimum value and the point at which the melting front reaches the right boundary and apply the scaling relationships described in Eqs. (10), (11), (12) and (14). Fig. 8 shows that the numerical results are in very good agreement with the scaling laws and enable us to extract the constants of proportionality. We added the results obtained by Jany and Bejan (1988) for $St = 0.1$ in Fig. 8b for comparison. The correlations we obtained (within a few percent) at $Pr = 1$ and $St = 10$ are listed in Table 2 together with the results of Jany and Bejan (1988).

Interestingly, the correlations for the time θ reported here are greater than those of Jany and Bejan (1988) by a factor five, while Nu correlations are in good agreement. From the scaling relations, a possible explanation is that the scaling laws derived for low St have to be corrected for the relatively large St we used. One way to understand this difference is by taking a closer look at the $Nu - \theta$ scaling at short times (when conduction is dominating the heat transfer). The Neumann solution for purely conductive melting leads to

$$Nu = \frac{1}{\text{erf}(\lambda)}(\pi Fo)^{-1/2} \tag{39}$$

in the limit of small St this can be simplified to

$$Nu = (2\theta)^{-1/2}. \tag{40}$$

A simple calculation shows that Eq. (40) underestimates the temporal evolution of the Nusselt number by a factor of approximately three for $St = 10$, and thus the high St will tend to shift Nu to higher θ. For example, Jany and Bejan (1988) propose the following correlation for the Nusselt number evolution (at low St):
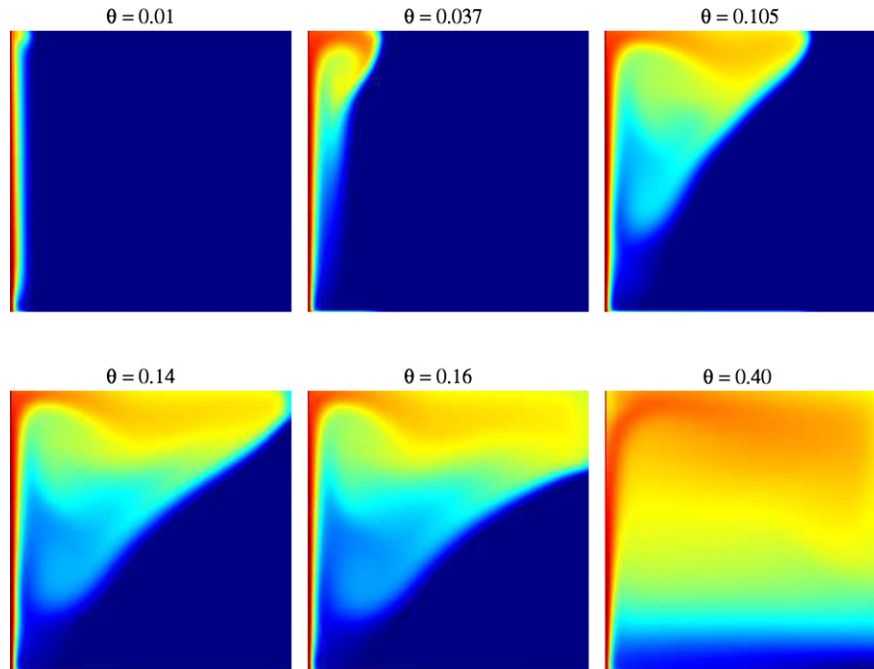
Fig. 6. Plot of the temperature field for different dimensionless times (θ). $Ra = 6.8 \times 10^6$, $Pr = 1$ and $St = 10$.
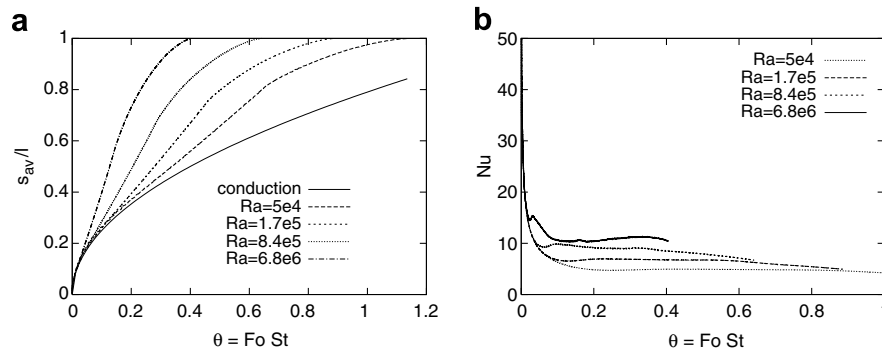

Fig. 7. (a) Average melting front position as function of dimensionless time θ for four different numerical runs, $Pr = 1$ and $St = 10$ for all. (b) Nusselt number evolution for four different numerical runs, $Pr = 1$ and $St = 10$ for all.
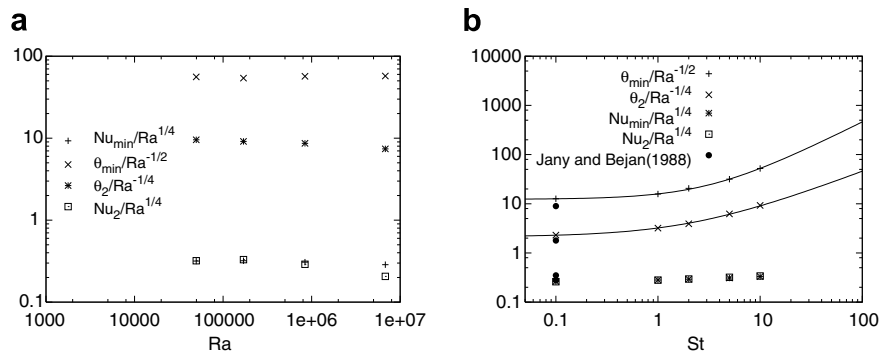

Fig. 8. Scalings from the numerical modeling. (a) Fixed $Pr = 1$ and $St = 10$. (b) Fixed $Pr = 1$ and $Ra = 10^5$. The two fits give $\theta_{min}/Ra^{-1/2} = 3.57St^{1.05} + 12.3$ and $\theta_2/Ra^{-1/4} = 1.1St^{0.8} + 2.12$.

Table 2
Comparison of the correlations obtained in this study ($St = 10$) with those of Jany and Bejan ($St = 0.1$)

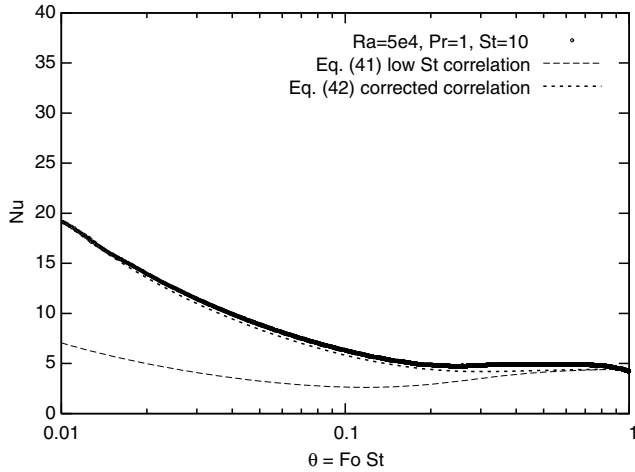|	Nu_{min}	θ_{min}	Nu_2	θ_2
Jany and Bejan (1988)	$0.28\ Ra^{1/4}$	$9\ Ra^{-1/2}$	$0.35\ Ra^{1/4}$	$1.8\ Ra^{-1/4}$
This study $St = 10$	$0.31\ Ra^{1/4}$	$56\ Ra^{-1/2}$	$0.29\ Ra^{1/4}$	$8.7\ Ra^{-1/4}$

Fig. 9. Comparison between numerical results and the correlation function from Eq. (41) and its corrected version for high St. In both cases, the fit was improved by replacing $c_2 = 0.0175$ by $c_2 = 0.00175$.

$$Nu = (2\theta)^{-1/2} + \left[c_1 Ra^{1/4} - (2\theta)^{-1/2}\right]\left[1 + (c_2 Ra^{3/4}\theta^{3/2})^n\right]^{1/n}, \quad (41)$$

where the constant $c_1 = 0.29$ is derived from the correlation of Nu_2 with $Ra^{1/4}$, c_2 and n are fitting parameters (they found $c_2 = 0.0175$

and $n = -2$). Here we propose a better correlation for the evolution of the Nusselt number by replacing each occurrence of $(2\theta)^{-1/2}$ by (39) in Eq. (41):

$$Nu = \frac{1}{\text{erf}(\lambda)}(\pi Fo)^{-1/2}$$
$$+ \left[c_1 Ra^{1/4} - \frac{1}{\text{erf}(\lambda)}(\pi Fo)^{-1/2}\right]\left[1 + (c_2 Ra^{3/4}\theta^{3/2})^n\right]^{1/n}. \quad (42)$$

We find that the fit is much improved (see Fig. 9), suggesting that the scalings for θ_{min} and θ_2 are not exactly independent of St (especially at high St). Other consequences of thermal inertia will be discussed later. To summarize the results at high St number, we observed that the scaling relations of Section 2 are in good agreement with our numerical results, and, the correlations for Nu_{min} and Nu_2 are very close to those observed by Jany and Bejan (1988), although the temporal position of these characteristic points is shifted to higher values of θ which seems to be consistent with the higher St used in our runs.

In order to validate the results we obtain from our lattice Boltzmann model, we compare the results of a numerical calculation made by Jany and Bejan (1988) (estimated from graphs in their paper) with $Ra = 1 \times 10^5$, $Pr = 50$ and $St = 0.1$ with a run with our scheme at similar Ra and St and slightly lower Pr (=5). According to the scaling laws (Jany and Bejan, 1988) and experimental results (Gobin and Bénard, 1992), at $Pr > 1$, the relationship between the Nusselt number and the Rayleigh number are independent of the Prandtl number, therefore the difference in Pr number between the two runs should not affect the comparison. Fig. 8b shows the constants we obtain for the scaling laws at $St = 0.1$; they are in good agreement with the results obtained by Jany and Bejan (1988).

Thermal inertia effects due to large superheat (high St number) have been introduced theoretically by Jany and Bejan (1988),
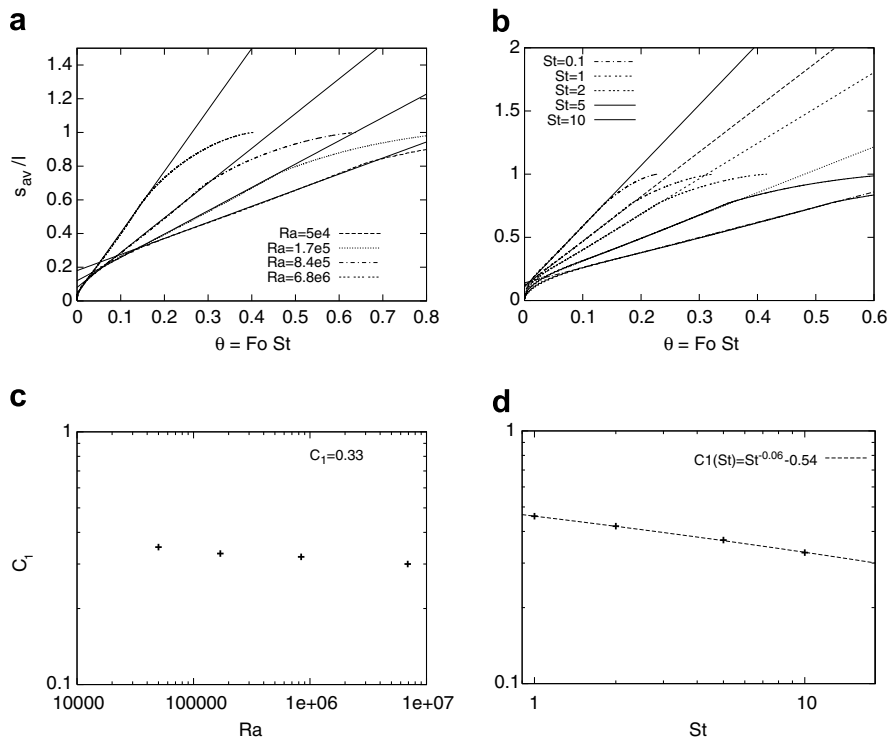

Fig. 10. Correlation for the thermal inertia effect using the scaling relation $ds_{av}/d\theta = 0.29 Ra^{1/4}/(1 + C_1 St)$. (a) $St = 10$ and $Pr = 1$; C_1 obtained from these correlations is 0.33 ± 0.02. (b) $Ra = 1 \times 10^5$ and $Pr = 1$; C_1 ranges from 0.33 to 0.46. The slopes of the straight lines, given by Eq. (44), match the numerical results during the fully-developed convection stage. (c) C_1 as function of Ra for $Pr = 1$ and $St = 10$. (d) C_1 as function of St for $Ra = 10^5$ and $Pr = 1$.

where they derive an expression for the propagation of the average melting front position during the fully developed convection stage

$$\frac{ds_{av}}{d\theta} = \frac{c_1 Ra^{1/4}}{1 + C_1 St},$$

(43)

where $c_1 = 0.29$ and C_1 is the constant incorporating thermal inertia effects into the melting front propagation. Fig. 10a shows the best fit from Eq. (43) and the corresponding values for C_1 are listed in Fig. 10c as a function of Ra ($St = 10$). Figs. 10b and d show the dependence of C_1 on the Stefan number. The best fits obtained from Eq. (43) for the melting front propagation during the fully convective regime (see Fig. 10b) lead to the values shown in Fig. 10d. As conjectured by Jany and Bejan (1988), we can confirm that C_1 is independent of the Stefan number over the range of Stefan number explored. Therefore, the evolution of the melting front in the fully-developed convection regime is best represented by the equation

$$\frac{ds_{av}}{d\theta} = \frac{c_1 Ra^{1/4}}{1 + 0.33 St},$$

(44)

for $5 \times 10^4 \leqslant Ra \leqslant 7 \times 10^6$ and $0.1 \leqslant St \leqslant 10$.

Suga (2006) showed that the conventional D2Q5 advection–diffusion scheme is stable for the condition $C_x^2 + C_y^2 \leqslant 2/5$ for $1 < \tau_h \leqslant 4$, where $C_x = u_x \delta_t / \delta_x$, $C_y = u_y \delta_t / \delta_y$ are the Courant numbers in the x and y directions, respectively. For low relaxation times ($\tau_h \sim 0.502$), the advection–diffusion scheme is stable for $\max(|C_x|, |C_y|) \leqslant 2/5$. The additional term accounting for the latent heat released, in our temperature scheme, brings an additional constraint on the Stefan number for the stability of the scheme (see Eq. (34)). However, these two stability constraints are not independent, and stability problems can still occur for large simulations at both high Ra and Pr. Stability can be recovered in these cases by reducing the duration of the time steps at the expense of computational time. Finally, Suga (2006) showed that the accu-
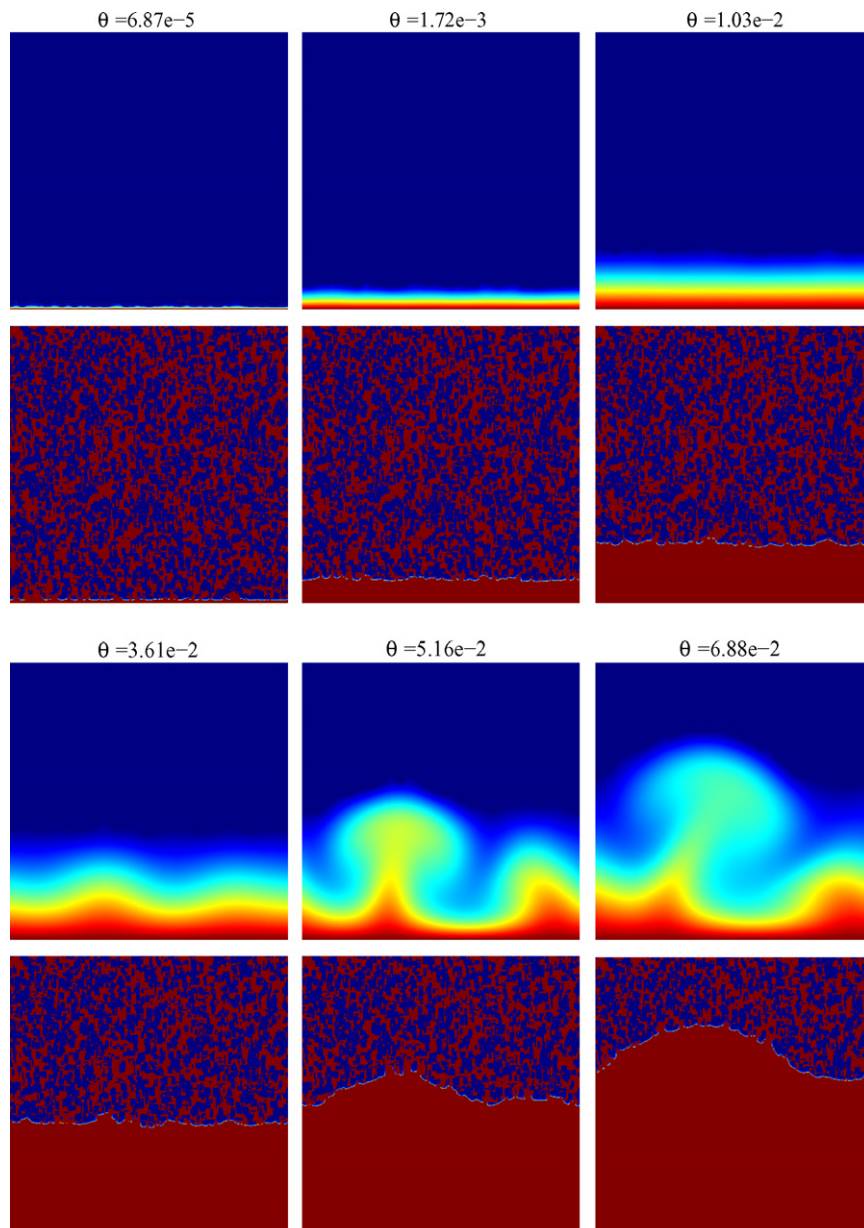

Fig. 11. Porous media convection melting. For each θ, two plots are shown, the temperature field in the upper row and the melt fraction in the lower row (where blue represents the solid). (For interpretation of the references to color in this figure legend, the reader is referred to the web version of this article.)

racy of the D2Q5 model for advection–diffusion problems depends mostly on the Peclet number ($Pe = u\delta_x/\kappa$), with a good accuracy when $Pe < 10$. All the numerical results presented in this study were well within the stability range of the D2Q5 model and performed at $Pe < 1$. We have tested different grid sizes and found that the appropriate grid size is limited by the stability and accuracy of the scheme at very low relaxation times (~ 0.501) for small grids and by the computational time for very large grids. Within this range, which depends on Ra, Pr and St, we find a good agreement between the different runs.

The model we describe in this study can solve for melting in porous media without modification. Convection melting in complex geometries (porous media) have many application in geosciences. For example, in volcanic settings, magma chambers host complicated dynamics with coexisting solid and liquid phases (as well as gas phases in general). Magmatic systems experience a complex temporal evolution with successive stages of reheating (related to injection of new magma for example) and cooling, resulting in a corresponding complex evolution of the local melt fraction by either melting or solidification. High energy reheating events are invoked to explain several eruptions of systems with relatively high crystallinity (around 40–50%) (Bachmann and Bergantz, 2003, 2006).

We apply our lattice Boltzmann convection melting model to a simulation of pure substance melting in a synthetic porous media (porosity of 45%). We use a 400×400 grid, the thermal diffusivity and the viscosity are set, respectively, to 1/3 and 1/6 in lattice units. Results are shown in Fig. 11. The domain is heated from below at a fixed temperature (above the melting temperature), the side walls are treated as periodic boundaries (for both temperature and fluid distributions) and the top wall is set as a no-slip, fixed temperature (melting temperature) boundary. The simulation is set with $Pr = 0.5$ and $St = 1.3$ (arbitrary choice). The systems melts from bottom up until it reaches a critical average height that enables large scale convection (at around $\theta = 3.6 \times 10^{-2}$). After this point, the melting rate is dominated by convection. The average pore-size is small enough to block convection beyond the melting front. In contrast with the Stefan problem, the melting front boundary is not flat because of horizontal temperature gradients due to the inhomogeneous distribution of the solid.

5. Conclusions

Lattice Boltzmann models offer a simple and powerful alternative to classic numerical methods when dealing with reactive flow in complex geometries. In this study, we present an explicit lattice Boltzmann scheme that can solve conduction and convection melting problems over a wide range of dimensionless parameters (especially Ra and St). Results show good agreement with scaling laws obtained by Jany and Bejan (1988). This approach also allows us to extend the scaling for the evolution of Nusselt number. In particular, our results suggest that the correlation developed by Jany and Bejan (1988) for the small St limit can be modified and generalized to $St > 1$. The correlation between the propagation of the melting front and the Stefan number during the fully developed convection regime is also established. We also show that the model presented here permits, without any subsequent modification, a study of convection melting in porous media.

References

Ansumali, S., Karlin, I., 2002. Single relaxation time model for entropic lattice Boltzmann methods. Phys. Rev. E 65 (5), 05631.

Bachmann, O., Bergantz, G.W., 2003. Rejuvenation of the Fish Canyon magma body: a window into the evolution of large-volume silicic magma systems. Geology 31, 789–792.

Bachmann, O., Bergantz, G.W., 2006. Gas percolation in upper-crustal magma bodies as a mechanism for upward heat advection and rejuvenation of silicic crystal mushes. J. Volcanol. Geotherm. Res. 149, 85–102.

Bénard, C., Gobin, D., Martinez, F., 2006. Melting in rectangular enclosures:experiments and numerical simulations. J. Heat Transf. 107, 794–803.

Bertrand, O., Binet, B., Combeau, H., Couturier, S., Delannoy, Y., Gobin, D., Lacroix, M., Le Quéré, P., Médale, M., Mencinger, J., Sadat, H., Vieira, G., 1999. Melting driven by natural convection. A comparison exercise: first results. Int. J. Therm. Sci. 38, 5–26.

Bodenschatz, E., Pesch, W., Ahlers, G., 2000. Recent developments in Rayleigh–Bénard convection. Annu. Rev. Fluid Mech. 32, 709–778.

Boettinger, W.J., Warren, J.A., Beckermann, C., Karma, A., 2002. Phase-field simulation of solidification. Annu. Rev. Mater. Res. 32, 163–194.

Chatterjee, D., Chakraborty, S., 2005. An enthalpy-based lattice Boltzmann model for diffusion dominated solid–liquid phase transformation. Phys. Lett. A 341, 320–330.

Chopard, B., Droz, M., 1998. Cellular Automata and Modeling of Physical Systems. Monographs and Texts in Statistical Physics. Cambridge University Press. p. 353.

Dong, Z.F., Chen, Z.Q., Wang, Q.J., Ebadian, M.A., 1991. Experimental and analytical study of contact melting in a rectangular cavity. J. Thermophys. 5, 347–354.

Faghri, A., Zhang, Y., 2006. Transport Phenomena in Multiphase Systems. Elsevier. p. 1030.

Frisch, U., Hasslacher, B., Pomeau, Y., 1986. Lattice gas automata for the Navier–Stokes equations. Phys. Rev. Lett. 56, 1505–1508.

Gobin, D., Bénard, C., 1992. Melting of metals driven by natural convection in the melt: influence of Prandtl and Rayleigh numbers. J. Heat Transf. 114, 521–524.

Guo, Z., Shi, B., Wang, N., 2000. Lattice BGK model for incompressible Navier–Stokes equation. J. Comput. Phys. 165, 288–306.

Guo, Z., Shi, B., Zheng, C., 2002. A coupled lattice BGK model for the Boussinesq equations. Int. J. Numer. Methods Fluids 39 (5), 325–342.

Guo, Z., Zhao, T.S., 2005. Lattice Boltzmann simulation of natural convection with temperature-dependent viscosity in a porous cavity. Progr. Comput. Fluid Dyn. 5, 110–117.

Hirata, T., Makino, Y., Kaneko, Y., 1993. Analysis of natural convection melting inside isothermally heated horizontal rectangular capsule. Wärme Stoffübertrag. 28, 1–9.

Hirt, C.W., Nichols, B.D., 1981. Volume of fluid (VOF) method for the dynamics of free boundaries. J. Comput. Phys. 39, 201–225.

Javierre, E., Vuik, C., Vermolen, F.J., van der Zwaag, S., 2006. A comparison of numerical models for one-dimensional Stefan problems. J. Comput. Appl. Math. 192, 445–459.

Jany, P., Bejan, A., 1988. Scaling theory of melting with natural convection in an enclosure. Int. J. Heat Mass Transf. 31, 1221–1235.

Jiaung, W.-S., Ho, J.-R., Kuo, C.-P., 2001. Lattice-Boltzmann method for the heat conduction problem with phase change. Numer. Heat Transf.: Part B 39, 167–187.

Kumar, R., Nivarthi, S.S., Ted Davis, H., Kroll, D.M., Maier, R.S., 1999. Application of the lattice-Boltzmann method to study flow and dispersion in channels with and without expansion and contraction geometry. Int. J. Numer. Methods Fluids 31, 801–819.

Lallemand, P., Luo, L.-S., 2003. Theory of the lattice Boltzmann method: acoustic and thermal properties in two and three dimensions. Phys. Rev. E 68, 036706.

Lätt, J., 2007. Hydrodynamic Limit of Lattice Boltzmann Equations, PhD Thesis, University of Geneva, p. 102.

McNamara, G., Alder, B., 1993a. Analysis of the lattice Boltzmann treatment of hydrodynamics. Physica A 194 (5), 218.

McNamara, G., Alder, B., 1993b. Lattice Boltzmann thermohydrodynamics. Phys. Rev. E 47 (4), 2249–2252.

Medvedev, D., Kassner, K., 2005. Lattice Boltzmann scheme for crystal growth in external flows. Phys. Rev. E 72, 056703.

Mencinger, J., 2004. Numerical simulation of melting in two-dimensional cavity using adaptive grid. J. Comput. Phys. 198, 243–264.

Mezrhab, A., Bouzidi, M., Lallemand, P., 2004. Hybrid lattice-Boltzmann finite-difference simulation of convective flows. Comput. Fluids 33, 623–641.

Miller, W., Succi, S., 2002. A lattice Boltzmann model for anisotropic crystal growth from melt. J. Stat. Phys. 112, 173–186.

Nourgaliev, R.R., Dinh, T.A., Dalal, D.C., Dinh, T.N., Theofanous, T.G., 2000. MuSiC: multiscale simulation code. modeling of complex fluid–fluid and fluid–solid interactions using the level-set and 'ghost fluid' methodology. Single- and Multiphase Compressible Flows, UCSB-CRSS Research Report, November 20, p. 209.

Nourgaliev, R.R., Dinh, T.N., Theofanous, T.G., Joseph, D., 2003. The lattice Boltzmann equation method: theoretical interpretation, numerics and implications. Int. J. Multiphase Flow 29, 117–169.

Prasianakis, N., Karlin, I., 2007. Lattice Boltzmann method for thermal flow simulation on standard lattices. Phys. Rev. E 76, 016702.

Qian, Y.H., D'Humières, D., Lallemand, P., 1992. Lattice BGK models for the Navier–Stokes equation. Europhys. Lett. 17, 479–484.

Rasin, I., Miller, W., Succi, S., 2005. Phase-field lattice kinetic scheme for the numerical simulation of dendritic growth. Phys. Rev. E 72, 066705.

Shan, X., 1997. Simulation of Rayleigh–Benard convection using a lattice Boltzmann method. Phys. Rev. E 55 (5), 2780–2788.

Succi, S., 2001. The lattice Boltzmann equation for fluid dynamics and beyond. Numerical Mathematics and Scientific Computation. Oxford University Press. p. 288.

Suga, S., 2006. Numerical schemes obtained from lattice Boltzmann equations for advection diffusion equations. Int. J. Mod. Phys. C 17 (11), 1563–1577.

Tan, L., Zabaras, N., 2006. A level set simulation of dendritic solidification with combined features of front-tracking and fixed-domain methods. J. Comput. Phys. 211, 36–63.

Usmani, A.S., Lewis, R.W., Seetharamu, K.N., 1992. Finite element modelling of natural-convection-controlled change of phase. Int. J. Numer. Methods Fluids 14, 1019–1036.

van der Sman, R.G.M., 2004. Diffusion on unstructured triangular grids using lattice Boltzmann. Future Gener. Comput. Syst. 20, 965–971.

van der Sman, R.G.M., 2006. Galilean invariant lattice Boltzmann scheme for natural convection on square and rectangular lattices. Phys. Rev. E 74, 026705.

Viskanta, R., 1982. Phase-change heat transfer. In: Lane, G.A. (Ed.), Solar Heat Storage: Latent Heat Materials. CRC Press, Boca Raton, FL, pp. 153–222.

Viskanta, R., 1985. Natural convection melting and solidification. In: Kakac, S., Aung, W., Viskanta, R. (Eds.), Natural Convection: Fundamentals and Applications. Hemisphere, Washington, DC, pp. 845–877.

Wang, Y., Amiri, A., Vafai, K., 1999. An experimental investigation of the melting process in a rectangular enclosure. Int. J. Heat Mass Transf. 42, 3659–3672.

Webb, B.W., Viskanta, R., 1986. Analysis of heat transfer during melting of a pure metal from an isothermal vertical wall. Numer. Heat Transf. 9, 539–558.

Wolff, F., Viskanta, R., 1987. Melting of pure metal from a vertical wall. Exp. Heat Transf. 1, 17–30.

Wolf-Gladrow, D.A., 2000. Lattice-Gas Cellular Automata and Lattice Boltzmann Models: An Introduction. Lecture Notes in Mathematics. Springer. p. 308.

Zhang, Z., Bejan, A., 1989. The problem of time-dependent natural convection melting with conduction in the solid. Int. J. Heat Mass Transf. 32, 2447–2457.